Article

Journal of
Nanoscience and Nanotechnology
Vol. 16, 196–202, 2016
www.aspbs.com/jnn

Molecular Imaging of CD44-Overexpressing Gastric Cancer in Mice Using T2 MR Imaging

Hwunjae Lee[1,2], Seung-Hyun Yang[1,2], Dan Heo[1,2], Heyoung Son[3], Seungjoo Haam[2,4], Jin-Suck Suh[1,2,3,5], Jaemoon Yang[1,5,*], and Yong-Min Huh[1,2,5,*]

[1]*Department of Radiology, College of Medicine, Yonsei University, Seoul, 120-752, Republic of Korea*
[2]*Nanomedical Interdisciplinary Program, National Core Research Center, Yonsei University, Seoul 120-749, Republic of Korea*
[3]*Severance Biomedical Science Institute, College of Medicine, Yonsei University, Seoul, 120-752, Republic of Korea*
[4]*Department of Chemical and Biomolecular Engineering, Yonsei University, Seoul 120-749, Republic of Korea*
[5]*YUHS-KRIBB Medical Convergence Research Institute, Seoul 120-752, Republic of Korea*

Novel diagnostic techniques have been developed in many research area using targetable contrast agents with magnetic resonance imaging (MRI) for cancer diagnosis. For cancer diagnosis, the use of MRI with biocompatible targeting moieties and manganese ferrite nanoparticles (MFNPs) is preferred. Thus, we synthesized MFNPs using a thermal decomposition method which enables sensitive T2 or T2 Turbo Spin Echo (TSE) MRI and coated them with hyaluronic acid (HA). The high targeting ability of HA-MFNPs was observed at MKN-45 cells (gastric cancer cell line) which high-expressing CD44 in contrast with MKN-28 cells which low-expressing CD44. We also prepared the gastric cancer mice model using MKN-45 cells which has the stem-like property was implanted into BALB/c nude mice. And then HA-MFNPs of the T2 contrast enhancement effects and targeting ability were investigated by *in vivo* MR imaging. As a result of these studies, we conclude that HA coated MFNPs can be effectively used as a novel probes for visualizing gastric cancer stem cells.

Keywords: Contrast Agent, Gastric Cancer, CD44, Magnetic Nanoparticles, Magnetic Resonance Imaging.

1. INTRODUCTION

Molecular imaging provides a tool to diagnose cancer at the cellular and molecular levels. It not only allows early and accurate tumor localization for diagnostic cancer imaging, but also has the potential to visualize the biological processes of tumor growth, metastasis, and response to treatment.[1–10] Molecular magnetic resonance (MR) imaging has emerged as a key tool in the diagnosis of cancer,[10–16] since it has advantages over noninvasive, anatomical imaging due to its high resolution, high contrast, and 3-dimensional information in real time, much more so than nuclear medicine (positron electron tomography and single-photon emission computed tomography) and optical imaging.[17–21] In addition, molecular MR imaging is able to simultaneously detect the metabolism of cells and tissues, physiological and structural information, and biological processes occurring in deep tissues.[22,23] Molecular MR imaging can be used to observe a variety of lesions in the diagnosis of gastric cancer but also has limitations.[24,25] In case of gastric cancer, it is difficult to diagnose using MR imaging because many foods and other digestive secretions exist inside the stomach.[24,26–29] Currently, many research groups are looking for a solution, but gastric cancer's limitations and difficulties can be addressed using various MR imaging contrast agents and MR sequence.

Many MR contrast agents have been used for good quality imaging.[13,30–34] However, the blood pool contrast agents cannot specifically reach their target goals. Thus, we aim to develop a targetable contrast agent using hyaluronic acid.[35–41] In particular, hyaluronic acid is known to interact with the CD44 receptor, and gastric cancer is known to overexpress the CD44 receptor, a biomarker of cancer stem cells.[42–47] It is crucial for MR probes to target early gastric cancer from a diagnostic point of view. CD44 is important as a gastric cancer stem cell marker as it interacts with hyaluronic acid. hyaluronic

*Authors to whom correspondence should be addressed.

 1533-4880/2016/16/196/007 doi:10.1166/jnn.2016.11782

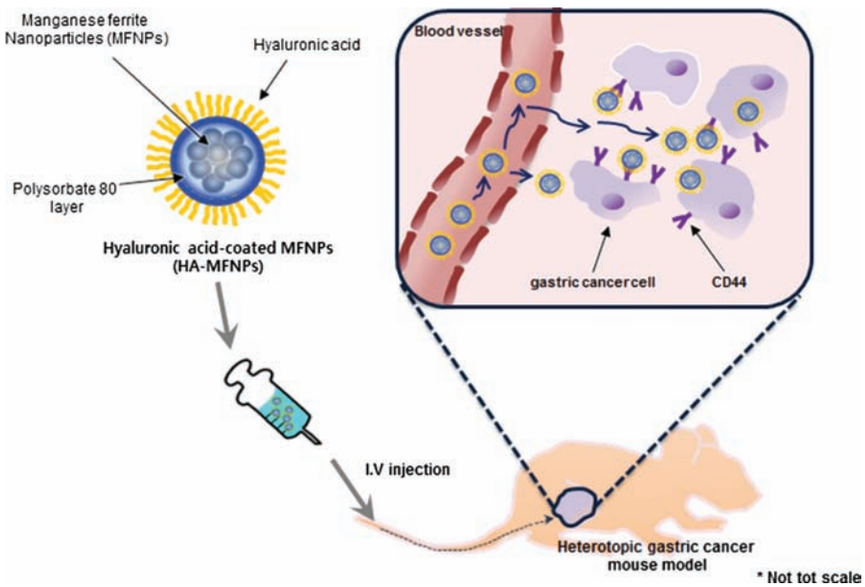

Scheme 1. Schematic illustration of hyaluronic acid-conjugated manganese ferrite nanoparticles (HA-MFNPs) for CD44-expressing gastric cancer cell-specific MR imaging

acid is a nontoxic, biocompatible polymer, with tandem disaccharide repeats of ß-1,4-D-glucuronic acid-ß-1,3-D-N-acetylglucosamine; components of the glycosaminoglycan family have been used in various areas as targeting moieties for MR probes as well as antibodies.[41,48–53] In addition, MRI sequence is also important in cancer diagnosis, In this study, molecular MR imaging was investigated to find biological processes that occur in gastric cancer. A T2 TSE sequence was used to confirm better diagnostic possibilities and targeting effects were demonstrated using hyaluronic acid-conjugated MFNPs (HA-MFNPs) in a heterotopic xenograft gastric cancer model (Scheme 1). Various experiments were conducted to evaluate specific binding affinity and diagnostic effectiveness both *in vivo* and *in vitro*.

2. EXPERIMENTAL DETAILS

2.1. Materials

Polysorbate 80 (P80), ethylenediamine, 1,4-dioxane (99.8%), and 1,1′-carbonyldiimidazole (CDI) were purchased from Sigma Aldrich Chemical Co. Phosphate buffered saline (PBS: 10 mM, pH 7.4), Roswell Park Memorial Institute-1640 (RPMI-1640), fetal bovine serum (FBS) and antibiotic-antimycotic solution were purchased from Gibco and dialysis membrane (1 kDa MWCO) from Spectrum laboratory. Hyaluronic acid (1 MDa) was supplied from Yuhan Phrmaceutical Corporation (Seoul, Korea). MKN-45 and MKN-28 (American Tissue Type Culture) cell lines were grown in medium containing 10% FBS and 1% antibiotic antimycotic at 37 °C and a humidified 5% CO_2 atmosphere. Ultrapure deionized water was used for all of the syntheses.

2.2. Synthesis of Manganese Ferrite Nanoparticles (MFNPs)

The monodispersed MFNPs were prepared by thermal decomposition method.[54] Briefly, 2 mmol iron (III) acetylacetonate, 1 mmol manganese (II) acetylacetonate, 10 mmol 1,2-hexadecanediol, 6 mmol dodecanoic acid, and 6 mmol dodecylamine were dissolved in 20 mL benzyl ether under an ambient nitrogen atmosphere. The mixture was then preheated to 200 °C for 2 h and refluxed at 300 °C for 30 min. After the reactants were cooled to room temperature, the products were purified with an excess of pure ethanol. Approximately 11 nm MFNPs were synthesized using the seed-mediated growth method.[55]

2.3. Preparation of HA-MFNPs

Aminated MFNPs were fabricated using the nanoemulsion method. First, 30 mg of MFNPs was dissolved in 4 ml of n-haxane (organic phase). The organic phase was injected into 30 ml of de-ionized water (aqueous phase) containing 100 mg of aminated P80. After mutual saturation, the solution was emulsified for 20 min under ultrasonification (ULH700S, Ulssohitech, Cheonwon-gum, South Korea) at 450 W. The mixture was kept overnight at room temperature to remove the volatile organic solvent. The product were purified using a centrifugal filter (Centriprep YM-3, 3-kDa molecular weight cutoff (MWCO), Amicon, Millipore Corporation, Billerica, MA, USA) in three times at 3,000 rpm for 20 min. HA-MFNPs were fabricated by EDC-NHS chemistry. First, the pH of the aminated MFNP solution was adjusted to neutral condition by the addition of 0.1 N HCl solution. Then, HA (9.63 μmol) were dissolved in the 40 ml of de-ionized water followed by the addition of EDC and sulfo-NHS.

Each HA solution was added to aminated MFNPs containing 50 mg of MFNPs. The HA and aminated MFNPs were reached for 2 h at room temperature. Finally, EDC, sulfo-NHS, and unbound HA were removed using dialysis (MWCO, 25,000) against excess de-ionized water. The hydrodynamic diameter and zeta potential of HA-MFNPs were analyzed by laser scattering (ELS-Z, Otsuka Electronics) and the relaxivity (R2) data of the HA-MFNPs was obtained by MR imaging analysis.

2.4. Biocompatibility Tests for HA-MFNPs

The cytotoxic effects of HA-MFNPs in MKN-45 cells and MKN-28 was evaluated by 3-(4,5- dimethylthiazol-2-yl)-2,5-diphenyltetrazolium bromide (MTT) assay. MKN-45 and MKN-28 cells were maintained in RPMI-1640 containing 10% FBS and 1% antibiotics at 37 °C in a humidified atmosphere with 5% CO_2. MKN-45 and MKN-28 cells (1.0×10^4 cells/well) were seeded into a 96-well plate at 37 °C overnight and the cells were incubated with various concentrations of HA-MFNPs for 4 h. The cells were washed with 100 μL PBS (pH 7.4, 1 mM), and 100 μL phenol red free RPMI-1640 was added. Subsequently, the cells were treated with MTT assay solution according to the manufacturer's instructions. Cell viability was evaluated using a microplate reader (Synergy H4 hybrid reader, BioTek) at an absorbance wavelength of 575 nm (reference wavelength of 650 nm). Cell viability was represented by normalization against HA-MFNPs-non-treated cells (which were considered as having 100% cell viability).

2.5. Darkfield Microscopy

MKN-45 and MKN-28 cells (2.0×10^5 cells/well) were seeded onto cover glass in 4 well plates and incubated at for 4 h at 37 °C. Prepared various concentrations of HA-MFNPs were added to RPMI. After incubation for 48 h at 37 °C, the cells were washed with PBS and fixed with 4% paraformaldehyde. To observe HA-MFNPs in the cells, the light scattering images were recorded using an inverted microscope (Olympus BX51, Japan) with a highly numerical darkfield condenser (U-DCW, Olympus), which delivers a very narrow beam of white light from a tungsten lamp to the surface of the sample. Immersion oil (nd: 1.516, Olympus) was used to narrow the gap between the condenser and the glass slide, and to balance the refractive index.

2.6. Prussian Blue Staining

MKN-45 and MKN-28 cells (1.0×10^6 cells/well) were seeded into 6-well plates and incubated at 37 °C. Prepared various concentrations of HA-MFNPs were mixed with RPMI-1640 and these mixtures were added to the cells. After incubation for 4 h at 37 °C, the cells were washed with PBS and fixed with 4% paraformaldehyde. The working solution was prepared by mixing 10% potassium ferrocyanide and 20% HCl in equal amounts. The working solution was added to the cells and incubated for 30 min at room temperature. The cells were washed with PBS and stained with nuclear fast red solution (Sigma, USA) for 30 min at room temperature. The cells were observed using an optical system microscope (Olympus BX51, Japan).

2.7. Heterotopic Animal Model and Experimental Procedure

All animal experiments were conducted with the approval of the Association for Assessment and Accreditation of Laboratory Animal Care (AAALAC) International. Female BALB/c nude mice at 7–8 weeks of age were anesthetized by intraperitoneal injection of a Zoletil/Rompun mixture and 1.0×10^7 MKN-45 cells which suspended in 200 μL saline were implanted into the femoral region. After cancer cell implantation, MR imaging was performed between 2 and 3 weeks. After *in vivo* MR imaging, MR imaging of the harvested organ was also performed. In addition, the extracted tumor tissues from tumor-bearing mice treated with HA-MFNPs were frozen, sectioned, and stained using Prussian blue. All stained tissue sections were analyzed using a virtual microscope (Olympus BX51, Japan) and Olyvia software.

2.8. MR Imaging

We performed solution and *in vitro* MR imaging experiments with a 1.5 T clinical MRI instrument with a micro-47 surface coil (Intera, Philips Medical Systems, Best, The Netherlands). The R2 (T2 relaxation rate, 1/T2, s^{-1}) of the HA-MFNPs solution and HA-MFNPs-treated cells (1×10^7) were measured by using the Carr-Purcell-Meiboom-Gill (CPMG) sequence at room temperature with the following parameters: TR = 10 sec, 32 echoes with 12 msec even echo space, number of acquisitions = 1, point resolution of 156×156 μm, and section thickness of 0.6 mm. For the acquisition of T2-weighted MR images of MFNPs solution and HA-MFNPs or HA-MFNPs-treated cells, the following parameters were adopted: resolution of 234×234 μm, section thickness of 2.0 mm, TE = 15 msec, TR = 400 msec, and number of acquisitions = 1. The $r2$ (mM^{-1} s^{-1}) is equal to the ratio of the R2 to the HA-MFNPs concentration. And *in vivo* MR imaging experiments were performed with a 3T Siemens clinical MR imaging instrument using a human wrist coil with T2 TSE sequence (TR: 4,000 ms, TE: 114 ms, slice thickness: 1.0 mm, FOV read: 180 mm).

3. RESULTS AND DISCUSSION

3.1. Preparation of MFNPs and HA-MFNPs

To detect the target cancer cells in MR images using low dose of contrast agent, the contrast agent should have the

high magnetic susceptibility. Thus, we synthesized high crystalline MFNPs ($MnFe_2O_4$) by the thermal decomposition method as previously reported.[54] It was reported that the relaxivity coefficient of $MnFe_2O_4$ is approximately 150% larger than Fe_3O_4.[57] The targeting moiety is also necessary for target specific MR imaging, thus we selected hyaluronic acid to targeting CD44-overexpressed gastric cancer cells. For the conjugation with hyaluronic acid, the MFNPs were enveloped by aminated P80 using nano-emulsion method. HA-MFNPs were synthesized using EDC/sulfo-NHS cross-linker. The hydrodynamic diameter of the aminated MFNPs and HA-MFNPs were determined to be 76.0 ± 18.5 nm and 132.4 ± 33.4 nm, respectively (Fig. 1(a)). In addition, the surface charge of the aminated MFNPs also changed from 21.2 ± 1.1 mV to -15.9 ± 1.2 mV after conjugation of hyaluronic acid due to the negative charge of carboxyl group of hyaluronic acid (Fig. 1(a)). After the conjugation of hyaluronic acid and the aminated MFNPs, the size slightly increased due to the large molecular weight of hyaluronic acid (1 MDa). The zeta potential was changed from the positive to negative after conjugation of hyaluronic acid because of the negative charge of carboxyl structure of hyaluronic acid.

As shown in Figure 1(b), the characteristic band of HA-MFNPs conjugates were verified by FT-IR spectra, which exhibits O–H stretching at 3200–3400 cm^{-1}, C=O stretching at 1100–1300 cm^{-1}, CO–NH(amide) bonds at 1630–1680 cm^{-1} and CH_2 bending in HA at 1430–1470 cm^{-1}. To assess the potential use of HA-MFNPs as MR imaging agents, we performed MR imaging analysis using HA-MFNPs, which exhibited the highest magnetic properties at the appropriate size to avoid reticuloendothelial system detection and prolong retention in the circulation. In Figure 1(d), the T2-weighted MR image exhibited a strong black color, which signified a decrease in signal intensity for the thicker HA-MFNPs solution.

3.2. *In Vitro* Analysis of HA-MFNPs

The MTT assay was then performed, in which yellow tetrazolium salt is reduced to purple formazan crystals in metabolically active cells. The relative percentage of cell viability was determined as the ratio of formazan intensity in viable cells which treated with HA-MFNPs to the intensity in non-treated (control) cells. As shown in Figure 1(c), the *in vitro* cytotoxicity measured by MTT assay showed that the viability of MKN-45 and MKN-28 cells was 80% at a concentration of 4.1 μg Fe + Mn/mL in HA-MFNPs.

For verifying specific targeting efficacy of HA-MFNPs, darkfield microscopy and Prussian blue staining analysis were carried out and MKN-45 (CD44 +) and MKN-28 (CD44 −) cell lines were selected due to difference of their CD44-expressing level. In Figure 2(a), darkfield microscopy images demonstrated that HA-MFNPs displayed excellent binding to MKN-45 cells in comparison with MKN-28 cells.

MKN-45 cells treated with HA-MFNPs exhibited bright spots. Furthermore, MKN-28 cells treated with HA-MFNPs exhibited a low number of bright spots, indicating that cellular binding affinity was low. Darkfield microscopy method is excluding the unscattered beam from image. As a result, the field around the specimen is generally dark. However, nanoparticles under same

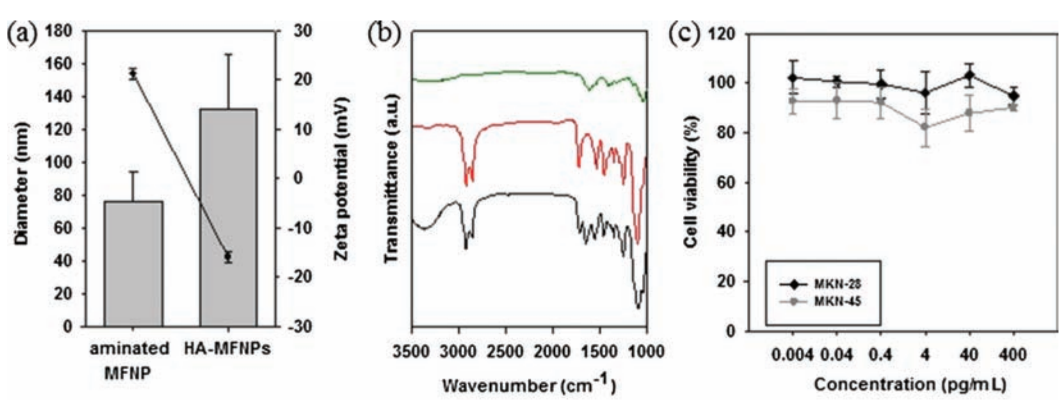

(d)

Fe concentration (mM)	0.0543	0.1085	0.2171	0.4342	0.8684
R2 (sec^{-1})	0.8495	0.9695	1.1521	1.5783	3.0769
MR image					

Figure 1. Characterization of HA-MFNPs for molecular MR imaging. (a) Hydrodynamic diameter (gray bar) and zeta potential (black circle) of aminated manganese ferrite nanoparticles (aminated MFNPs) and hyaluronic acid-conjugated MFNPs (HA-MFNPs), respectively. (b) Fourier transform infrared spectra of HA (green line), MFNPs (red line) and HA-MFNPs (black line). (c) Cell proliferation assay of MKN-28 (CD44 −), MKN-45 (CD44 +) cells after treatment of HA-MFNPs at several concentrations. (d) Table of R2 values and MR images for each Fe concentration of HA-MFNPs.

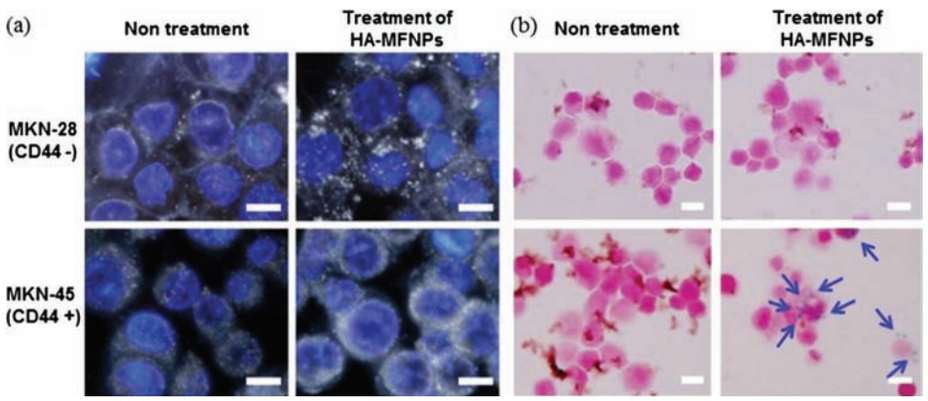

Figure 2. *In vitro* microscopic analysis of MKN-28 (CD44 −) and MKN-45 (CD44 +) cells after treatment of HA-MFNPs. (a) darkfield microscopic images of MKN-28 (CD44 −), MKN-45 (CD44 +) cells were incubated with 10 μg/mL of HA-MFNPs in 4 h. (b) prussian blue staining images of MKN-28 (CD44 −), MKN-45 (CD44 +) cells were treated with 40 μg/mL of HA-MFNPs in 4 h. All scale bars are 5 μm.

brightness were scattered more than cellular matrix, thus they shine brightly like a white spots.

In Figure 2(b), the extent of intracellular uptake of HA-MFNP in both MKN-45 and MKN-28 cells was confirmed using microscopic images after Prussian blue staining. Prussian blue staining is a commonly used in histopathology to detect the presence of iron in specimens. Any ferric ion present in the specimens combines with the ferrocyanide and results in the formation of a bright blue color. As a result, one can confirm the presence of a small

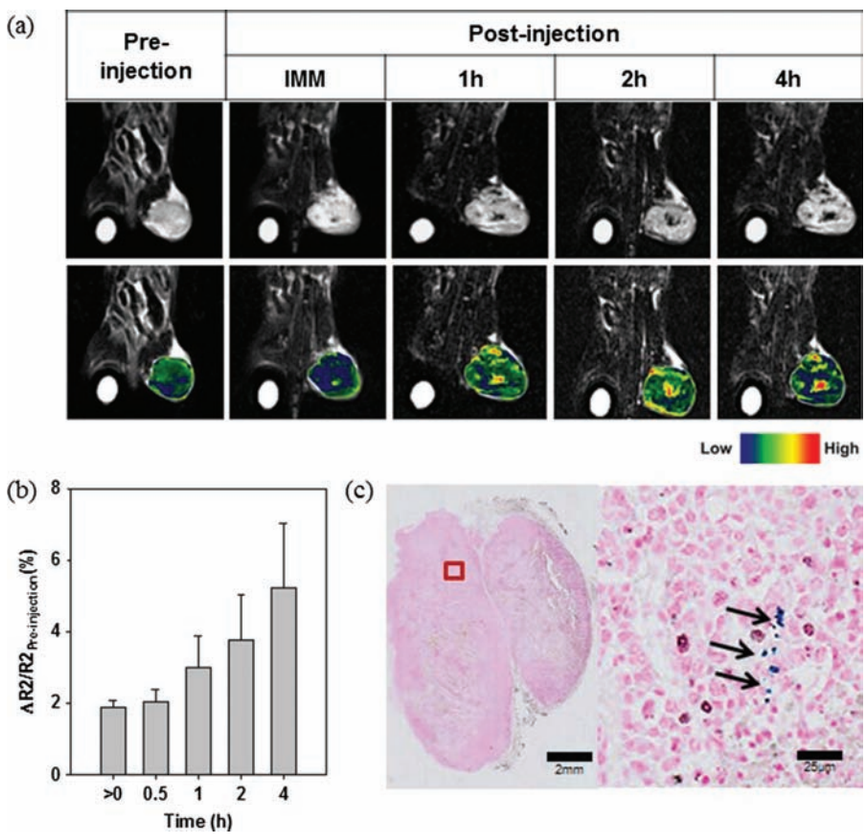

Figure 3. *In vivo* MR imaging of MKN-45 xenograft mouse model and histological analysis. (a) T2 TSE MR images of xenograft mouse model after intravenous injection of HA-MFNPs. TR: 4,000 ms, TE: 114 ms, Slice thickness: 1.0 mm, FOV read: 180 mm, coil elements: wrist coil. (b) $\Delta R2/R2_{Pre\text{-}injection}(\%)$ graph verses time after intravenous injection of HA-MFNP respectively. (c) Prussian blue staining image of tumor in mouse xenograft model. Right pictures are magnified image of 80 times from left.

amount of iron contained in the nanoparticles in cells or tissues. The transport of HA-MFNPs into MKN-45 cells took place efficiently. In contrast, MKN-45 and MKN-28 cells treated with HA-MFNPs exhibited insignificant cellular uptake. The small fractions of observed iron were represented the nonspecific cellular binding of MFNPs.

3.3. *In Vivo* MR Imaging Analysis of HA-MFNPs

The xenograft mice model were prepared to heterotopic tumor model, thus MKN-45 cells were implanted into right thigh intrasubcutanously because it has some advantages to observe the volume or morphology of the tumor rather than orthotopic gastric cancer model. In Figure 3, contrast enhancement in MR imaging was identified after HA-MFNPs injection into xenograft mice model. In T2 TSE MR images, clear anatomic details were observed, and there was no artifact due to a difference in susceptibility. Initially, the center of the tumor instantly darkened, and contrast enhancement at surrounding vessels was simultaneously observed (Fig. 3(a)). Four hours after intravenous injection of HA-MFNPs into the lateral tail vein of the mice model, the T2-contrast enhancement was observed at the tumor site. In contrast, in the MR image of post-injection 30 min, the change of T2-signal was not shown significantly. This result was re-confirmed $\Delta R2/R2_{\text{Pre-injection}}(\%)$ graph. We think this data demonstrate that the HA-MFNPs have the ability of long circulation against of other T1 contrast agent.

3.4. Histological Analysis

In Figure 3(c), the histological morphology of tumor was confirmed using H&E staining. We noticed that each of the cancer cells could be observed through hematoxylin (nucleus: blue) and eosin Y (cytoplasm: pink) staining. Figure 3(c) shows that the iron content (black arrows) of accumulated HA-MFNPs in the tumors was also observed by Prussian blue staining. We thus confirmed that our developed HA-MFNPs had an adequate capability for targeting CD44-overexpressing gastric cancer.

4. CONCLUSIONS

In summary, we synthesized HA-MFNPs as MR imaging agents for effective diagnoses of CD44-overexpressing gastric cancer. Gastric cancer is difficult to diagnose using MR imaging, but we tried to solve this problem by using an HA-MNFP contrast agent. We plan to evaluate additional imaging tools using variable MR sequences for a better imaging technique.

Acknowledgments: This work was supported by the Nation Research Foundation grant (2006-2004652) funded by the Korea government (MEST)/grant from the National R&D Program for Cancer Control, Ministry for Health and Welfare, Republic of Korea (1220100)/the National Research Foundation of Korea (NRF) grant funded by the Korea government (MEST) (NRF-2014R1A1A2059806).

References and Notes

1. J. K. Kim, K. J. Choi, M. Lee, M. H. Jo, and S. Kim, *Biomaterials* 33, 207 (**2012**).
2. M. F. Kircher, H. Hricak, and S. M. Larson, *Molecular Oncology* 6, 182 (**2012**).
3. X. Meng, B. W. Loo, Jr., L. Ma, J. D. Murphy, X. Sun, and J. Yu, *The J. of Nuclear Medicine: Official Publication, Society of Nuclear Medicine* 52, 1573 (**2011**).
4. P. Gong, B. Shi, M. Zheng, B. Wang, P. Zhang, D. Hu, D. Gao, Z. Sheng, C. Zheng, Y. Ma, and L. Cai, *Biomaterials* 33, 7810 (**2012**).
5. R. G. Blasberg, *Molecular Cancer Therapeutics* 2, 335 (**2003**).
6. J. M. Hoffman and A. E. Menkens, *Academic Radiology* 7, 905 (**2000**).
7. J. Bzyl, W. Lederle, A. Rix, C. Grouls, I. Tardy, S. Pochon, M. Siepmann, T. Penzkofer, M. Schneider, F. Kiessling, and M. Palmowski, *European Radiology* 21, 1988 (**2011**).
8. M. Nishino, D. M. Jackman, H. Hatabu, P. A. Janne, B. E. Johnson, and A. D. Van den Abbeele, *Academic Radiology* 18, 424 (**2011**).
9. F. Kiessling, *Radiology* 256, 331 (**2010**).
10. K. Pinker, A. Stadlbauer, W. Bogner, S. Gruber, and T. H. Helbich, *European Journal of Radiology* 81, 566 (**2012**).
11. D. Artemov, N. Mori, B. Okollie, and Z. M. Bhujwalla, *Magnetic Resonance in Medicine: Official Journal of the Society of Magnetic Resonance in Medicine/Society of Magnetic Resonance in Medicine* 49, 403 (**2003**).
12. A. Gossmann, Y. Okuhata, D. M. Shames, T. H. Helbich, T. P. L. Roberts, M. F. Wendland, S. Huber, and R. C. Brasch, *Radiology* 213, 265 (**1999**).
13. M. Q. Tan, S. M. Burden-Gulley, W. Li, X. M. Wu, D. Lindner, S. M. Brady-Kalnay, V. Gulani, and Z. R. Lu, *Pharm Res-Dordr* 29, 953 (**2012**).
14. H. T. Song and J. S. Suh, *J. Korean Med. Assoc.* 52, 121 (**2009**).
15. N. Grenier, B. Quesson, B. D. de Senneville, H. Trillaud, F. Couillaud, and C. Moonen, *Jbr-Btr.* 92, 8 (**2009**).
16. A. Gossmann, Y. Okuhata, D. M. Shames, T. H. Helbich, T. P. Roberts, M. F. Wendland, S. Huber, and R. C. Brasch, *Radiology* 213, 265 (**1999**).
17. D. Thomas, H. Bal, J. Arkles, J. Horowitz, L. Araujo, P. D. Acton, and V. A. Ferrari, *Magnetic Resonance in Medicine: Official Journal of the Society of Magnetic Resonance in Medicine/Society of Magnetic Resonance in Medicine* 59, 252 (**2008**).
18. A. Coimbra, D. S. Williams, and E. D. Hostetler, *Current Topics in Medicinal Chemistry* 6, 629 (**2006**).
19. S. S. Spencer, W. H. Theodore, and S. F. Berkovic, *Magnetic Resonance Imaging* 13, 1119 (**1995**).
20. A. Y. Kim, J. K. Han, C. K. Seong, T. K. Kim, and B. I. Choi, *J. of Computer Assisted Tomography* 24, 389 (**2000**).
21. L. M. Portnoi, L. B. Denisova, G. A. Stashuk, and V. O. Nefedova, *Vestnik Rentgenologii I Radiologii* 1, 26 (**2000**).
22. M. Bradbury and H. Hricak, *Magnetic Resonance Imaging Clinics of North America* 13, 225 (**2005**).
23. E. J. Delikatny and H. Poptani, *Radiologic Clinics of North America* 43, 205 (**2005**).
24. I. M. de Zwart and A. de Roos, *European Radiology* 20, 2609 (**2010**).
25. M. Takeda, Y. Amano, T. Machida, S. Kato, Z. Naito, and S. Kumita, *Japanese Journal of Radiology* 30, 602 (**2012**).
26. T. Motohara and R. C. Semelka, *Abdominal Imaging* 27, 376 (**2002**)
27. M. E. Spieth and B. S. Gauger, *AJR. American Journal of Roentgenology* 182, 259 (**2004**).
28. C. J. Das, J. Debnath, and S. Mukhopadhyay, *Indian Journal of Gastroenterology: Official Journal of the Indian Society of Gastroenterology* 25, 81 (**2006**).

29. I. Y. Kim, S. W. Kim, H. C. Shin, M. S. Lee, D. J. Jeong, C. J. Kim, and Y. T. Kim, *World Journal of Gastroenterology: WJG* 15, 3992 (**2009**).
30. M. Buijs, I. R. Kamel, J. A. Vossen, C. S. Georgiades, K. Hong, and J. F. Geschwind, *Journal of Vascular, and Interventional Radiology* 18, 957 (**2007**).
31. J. Rydland, A. BjOrnerud, O. Haugen, G. Torheim, C. Torres, K. A. Kvistad, and O. Haraldseth, *Acta Radiol.* 44, 275 (**2003**).
32. K. Nikolaou, H. Kramer, C. Grosse, D. Clevert, O. Dietrich, M. Hartmann, P. Chamberlin, S. Assmann, M. F. Reiser, and S. O. Schoenberg, *Radiology* 241, 861 (**2006**).
33. C. P. Stracke, M. Katoh, A. J. Wiethoff, E. C. Parsons, P. Spangenberg, and E. Spuntrup, *Stroke; A Journal of Cerebral Circulation* 38, 1476 (**2007**).
34. N. McDannold, S. L. Fossheim, H. Rasmussen, H. Martin, N. Vykhodtseva, and K. Hynynen, *Radiology* 230, 743 (**2004**).
35. E. K. Lim, H. O. Kim, E. Jang, J. Park, K. Lee, J. S. Suh, Y. M. Huh, and S. Haam, *Biomaterials* 32, 7941 (**2011**).
36. Y. He, G. D. Wu, T. Sadahiro, S. I. Noh, H. Wang, D. Talavera, J. M. Vierling, and A. S. Klein, *American Journal of Physiology. Gastrointestinal, and Liver Physiology* 295, G305 (**2008**).
37. M. M. Knupfer, H. Poppenborg, M. Hotfilder, K. Kuhnel, J. E. Wolff, and M. Domula, *Clinical and Experimental Metastasis* 17, 71 (**1999**).
38. H. Miyake, I. Hara, I. Okamoto, K. Gohji, K. Yamanaka, S. Arakawa, H. Saya, and S. Kamidono, *The J. of Urology* 160, 1562 (**1998**).
39. J. Lesley and R. Hyman, *European Journal of Immunology* 22, 2719 (**1992**).
40. R. Hyman, J. Lesley, and R. Schulte, *Immunogenetics* 33, 392 (**1991**).
41. W. Zhang, L. Gao, S. Qi, D. Liu, D. Xu, J. Peng, P. Daloze, H. Chen, and R. Buelow, *Transplantation* 69, 665 (**2000**).
42. B. I. Jang, Y. Li, D. Y. Graham, and P. Cen, *Gut, and Liver* 5, 397 (**2011**).
43. C. S. Yong, C. M. Ou Yang, Y. H. Chou, C. S. Liao, C. W. Lee, and C. C. Lee, *BMC Gastroenterology* 12, 95 (**2012**).
44. C. Zhang, C. Li, F. He, Y. Cai, and H. Yang, *Journal of Cancer Research, and Clinical Oncology* 137, 1679 (**2011**).
45. N. Matsuura, H. Waki, A. Tsukiyama, and M. Tsujimoto, *Nihon Rinsho. Japanese Journal of Clinical Medicine* 59, 101 (**2001**).
46. H. F. Hsieh, J. C. Yu, L. I. Ho, S. C. Chiu, and H. J. Harn, *Molecular Pathology: MP* 52, 25 (**1999**).
47. A. Yamaguchi, M. Saito, T. Gio, A. Iida, K. Takeuchi, K. Hirose, G. Nakagawara, T. Urano, K. Furukawa, and H. Shiku, *Japanese Journal of Cancer Research: Gann* 86, 1166 (**1995**).
48. R. W. Moskowitz, *Current Rheumatology Reports* 2, 466 (**2000**).
49. M. Wiig and S. O. Abrahamsson, *J. Hand Surg. Br.* 25, 183 (**2000**).
50. R. N. Rosier and R. J. O'Keefe, *Instructional Course Lectures* 49, 495 (**2000**).
51. D. M. Schwartz, R. Equi, and M. Jumper, *Archives of Ophthalmology* 118, 445 (**2000**).
52. T. Kaneko, H. Saito, M. Toya, T. Satio, K. Nakahara, and M. Hiroi, *J. of Assisted Reproduction, and Genetics* 17, 162 (**2000**).
53. V. B. Lokeshwar, C. Obek, H. T. Pham, D. Wei, M. J. Young, R. C. Duncan, M. S. Soloway, and N. L. Block, *The J. of Urology* 163, 348 (**2000**)
54. J. Yang, L. C. H., K. H. J., S. J. S., Y. H. G., L. K., H. Y. M., and S. Haam, *Angew. Chem. Int. Edn* 46, 8836 (**2007**).
55. S. H. Yang, D. Heo, J. Park, S. Na, J. S. Suh, S. Haam, S. W. Park, Y. M. Huh, and J. Yang, *Nanotechnology* 23, 505702 (**2012**).
56. E.-K. Lim, J. Yang, J.-S. Suh, Y.-M. Huh, and S. Haam, *J. Mater. Chem.* 19, 8958 (**2009**).
57. J. H. Lee, Y. M. Huh, Y. W. Jun, J. W. Seo, J. T. Jang, H. T. Song, S. Kim, E. J. Cho, H. G. Yoon, J. S. Suh, and J. Cheon, *Nature Medicine* 13, 95 (**2007**).

Received: 19 January 2015. Accepted: 24 April 2015.